Spatiotemporal Variability in the Annual Sea Level Cycle Along the Global Coast

A. Barroso[1], T. Wahl[1], S. Li[2], A. Enriquez[1,3], J. Morim[1], S. Dangendorf[4], C. Piecuch[5], P. Thompson[6]

[1]Department of Civil, Environmental and Construction Engineering and National Center for Integrated Coastal Research, University of Central Florida, Orlando, FL, USA

[2]State Key Laboratory of Geodesy and Earth's Dynamics, Innovation Academy for Precision Measurement Science and Technology, Chinese Academy of Sciences, Wuhan, China

[3]Institute for Environmental Studies (IVM), Vrije Universiteit Amsterdam, Amsterdam, Netherlands

[4]Department of River-Coastal Science and Engineering, Tulane University, New Orleans, LA, USA

[5]Department of Physical Oceanography, Woods Hole Oceanographic Institution, Woods Hole, MA, USA

[6]Department of Oceanography, University of Hawai'i, Honolulu, HI, USA

Key Points:

- The annual sea level cycle is non-stationary and has changed by up to more than a month across multiple locations.
- There are well-defined regional clusters of tide gauges where the annual sea level cycle exhibits similar variability patterns.
- Changes in the annual sea level cycle are linked to dominant modes of climate variability.

Abstract

Changes in the seasonal sea level cycle (SSLC) can modulate the flooding risk along coastlines. Here, we use harmonic analysis to quantify changes in the amplitude and phase of the annual component of the sea level cycle at 663 tide gauge locations along the global coastline where long records are available. We identify coastal hotspots by applying clustering methods revealing coherent regions with similar patterns of variability in the annual sea level cycle (ASLC). Results show that for most tide gauges the annual amplitude reached its maximum after 1970 and its peak typically occurs during the fall season of the respective hemisphere. Many tide gauges exhibit non-stationarity in the annual cycle in terms of amplitude and/or phase. For example, at 125 tide gauges we find significant trends in the amplitude (either increasing or decreasing) while several sites (36 in total), mostly in the Mediterranean and around Pacific islands, experienced phase changes leading to shifts in the timing of the peak of the annual cycle by more than a month. Our results highlight the importance of accounting for potential non-stationarity in seasonal mean sea level (MSL) cycles along coastlines.

Plain Language Summary

The seasonal sea level cycle (SSLC) is the pattern of high and low mean sea level (MSL) observed throughout the year at a given location. Shifts in the timing of the maximum sea level impact coastlines with increased risk of flooding if the higher MSL occurs at a time of year when other factors like storms or high tides are also at their peak. To understand changes in the SSLC, we focus on the annual sea level cycle (ASLC) by decomposing the MSL at 663 locations into amplitude and phase components which describe the variability and timing of the MSL annual peak, respectively. We find that MSL amplitude typically reaches its maximum during the fall in each hemisphere. Coastal hotspots in the North Atlantic have been identified with coherent regions showing similar patterns in their ASLC variability. We find 125 locations with significant trends in amplitude and 36 locations where the MSL peak has changed by more than a month throughout the record. Additionally, we find significant relationships between the MSL annual amplitudes and climate indices characterizing regional-scale climate phenomena. Our results provide a comprehensive description of changes in the ASLC along portions of the global coastline with tide gauges.

1. Introduction

Many coastal locations worldwide have experienced the impacts of sea level change. This includes saltwater intrusion, freshwater resource contamination, ecosystem disruptions, surge propagation, coastal infrastructure damage, and other socio-economic impacts related to flooding, which are especially observable in low-lying areas (IPCC, 2023). In addition to projections of sea level changes, it is important to understand modulations of regular and predictable cycles of mean sea level (MSL). These can coincide with other natural climate processes or with components of extreme sea level, such as storm surge, to heighten the resulting

69 total sea level at a particular location (Wahl et al., 2014). For example, when the maximum MSL
70 for a given year aligns with a region's seasonal maximum of storm activity or with the seasonal
71 high tides (often referred to as king tides), the likelihood for flooding is relatively higher as
72 opposed to when the MSL peaks occur out of phase.

73 The seasonal sea level cycle (SSLC) describes the sea level pattern observed annually due to the
74 regional climate characteristics of a location. It can be represented by the sum of annual and
75 semi-annual harmonics with amplitudes and phases that correspond to the magnitude and timing
76 of monthly MSL maxima and minima. Changes in the amplitude over time lead to larger
77 differences between the troughs and peaks, while shifts in the phase can move the peak closer to
78 or away from the storm surge season. The SSLC is often assumed to be stationary in time and is
79 removed in studies considering sea level variability, but non-stationarity of the SSLC has been
80 found to play a significant role in contributing to coastal sea level variations (Feng et al. 2015).
81 The SSLC has been studied previously at the global scale (e.g., Gill & Niller 1973; Pattullo et al.
82 1955; Pugh & Woodworth, 2014; Vinogradov et al., 2008) and across specific regions worldwide
83 (e.g., Amiruddin et al., 2015; Barbosa et al., 2008; Barbosa & Silva, 2009; Calafat et al., 2018;
84 Dangendorf et al., 2012; 2013; Feng et al., 2015; Hünicke & Zorita, 2008; Marcos & Tsimplis,
85 2007; Plag & Tsimplis, 1999; Torres & Tsimplis, 2012; Wahl et al., 2014).

86 However, these studies either focused on the mean SSLC or assessed changes in individual
87 regions; changes of the SSLC over time in terms of amplitude and phase have not been
88 comprehensively assessed on a global scale. Here, our central aim is to analyze how the annual
89 component of the SSLC, hereafter referred to as the annual sea level cycle (ASLC), observed by
90 tide gauges globally has varied in space and time. We extend previous analyses (e.g., Wahl et al.,
91 2014; Calafat et al., 2018) to a broader scope of the global coastline and add investigations of the

annual phase component. We assess how much the amplitude and phase of the annual cycle has fluctuated around the mean in the past and identify recent trends. In this context, we also identify clusters of coherent variability in the annual amplitude for the North Atlantic coastlines, as an example, where we have a dense network of tide gauges. Finally, we compare relevant climate indices to the annual amplitudes to detect whether any significant relationships exist. By doing this, we provide a comprehensive description of spatiotemporal variability in the ASLC along gauged portions of the global coastline.

2. Data

Monthly MSL data measured by tide gauges was obtained from the Permanent Service for Mean Sea Level (PSMSL) database (Woodworth & Player, 2003; Holgate et al., 2013). The tide gauge data used are the revised local reference (RLR) subset. A total of 737 tide gauges located across the globe were chosen initially according to a minimum record length of 30 years. Since the focus of this study is on changes in the ASLC along the global coasts, 26 tide gauges were discarded based on locations in lakes, rivers, or near glaciers where the seasonal cycles of water levels are heavily influenced by different processes than the coastal ASLC (Amiruddin et al., 2015; Tsimplis & Woodworth, 1994) and hence outside the scope of this study. An additional 48 tide gauges were discarded after performing sensitivity analyses which revealed questionable data records (see Methods). This resulted in the final set of 663 tide gauges that are used to analyze the ASLC and its changes over time (see Figure 1 for the locations and record lengths). Additionally, climate indices were downloaded from the National Oceanic and Atmospheric Administration's Physical Sciences Laboratory (NOAA PSL). The indices used are: El Niño 3.4,

North Atlantic Oscillation (NAO), Atlantic Multidecadal Oscillation (AMO), and the Pacific Decadal Oscillation (PDO) because of their large-scale influence on climate.

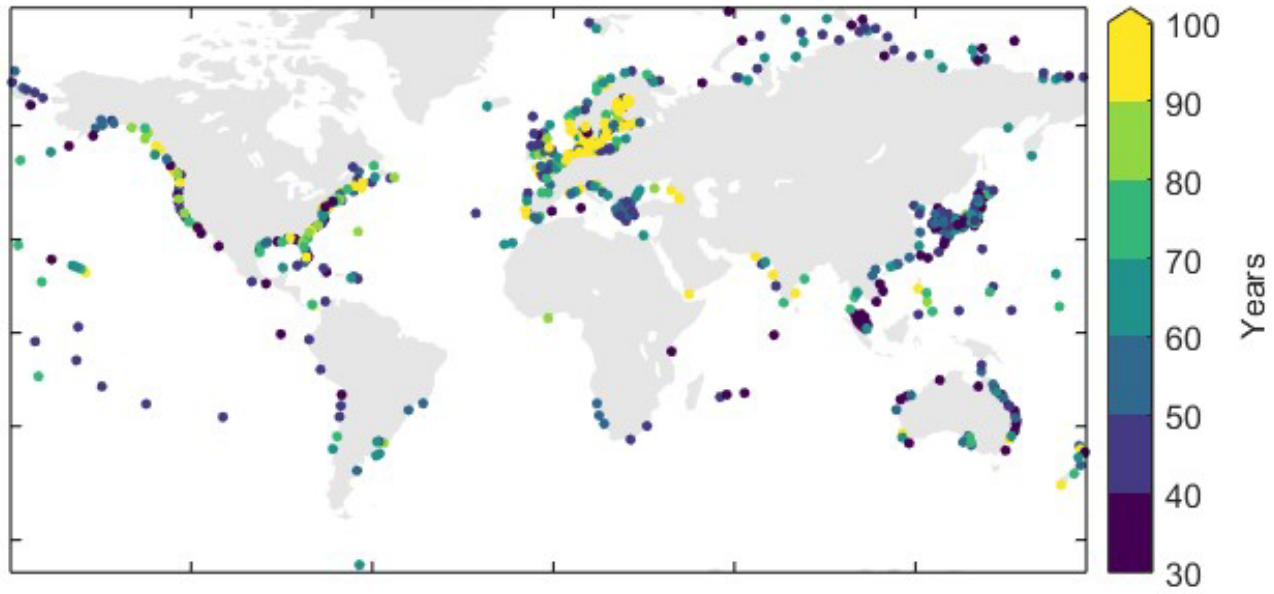

Figure 1. Number of years of monthly MSL data available from 663 tide gauges. Records longer than 100 years (72 tide gauges) are all shown in yellow.

3. Methods

3.1 Harmonic Analysis

Following Wahl et al. (2014), we perform a harmonic analysis to deconstruct the MSL into the components of interest. We fit a regression model to moving 5-year windows with no more than two years of missing data (also see Section 3.2) of the monthly MSL time series and shift the window by one month each time step, as has been done in previous studies (Tsimplis & Woodworth, 1994; Plag & Tsimplis, 1999; Amiruddin et al., 2015):

$$MSL(t) = MSL_0 + at + A_1 \cos[2\pi(t - p_1)] + A_2 \cos\left[\frac{2\pi}{0.5}(t - p_2)\right] \quad (1)$$

Equation 1 shows how the time changing MSL(t) is decomposed into six parameters: the MSL_0 (constant mean value) for the respective time window (where *t* is the time in years), a linear trend *a*, the annual and semi-annual amplitudes, A_1 and A_2, and the annual and semi-annual phase, p_1 and p_2. The harmonic constituents are estimated at the central month of each 5-year time window (i.e., 30th month). Therefore, there are no values during the first and last 30 months. The phases are extracted from the model and calculated based on trigonometric theory (Eq. 2) in reference to a fixed time frame, so that the degrees can be interpreted as months of the year. January is the starting point at 0 degrees. Each calendar month of the year increases by 30 degrees for the annual phase, reaching a total of 360 degrees by the end of December.

$$\text{Annual phase degree: } p_1 = \frac{(360^0)(nth\ day)}{365\ days} \quad (2)$$

3.2 Sensitivity Analysis

To assure robustness of our results, we perform different sensitivity tests. We compare Ordinary Least Squares (OLS) estimation to robust fit for deriving regression coefficients and we contrast the results against the Bayesian approach by Calafat et al. (2018) at select sites. We also apply jackknife resampling of the 5-year moving windows to assess how missing data (e.g., individual extreme years) can influence the results. Lastly, we test the precision of the phase estimates since our model returns phase degree values of daily resolution from monthly data.

3.2.1 Models: Ordinary Least Squares Estimation vs. Robust Fit

We compared OLS and robust fit to estimate regression parameters and found that the models produce different results in some locations. In most places results are similar, but to identify tide gauges where data inconsistencies could lead to larger differences and influence our results, we select locations with maximum RMSE > 0.8 cm between models and a difference > 3 cm in the

annual amplitude estimates. For some tide gauges where those thresholds are exceeded, we find vertical shifts due to earthquakes, e.g., in locations around Japan. We identify the change points and remove the years before or after datum shifts; if less than 30 years of consistent data are left, the tide gauges are discarded. In other places like the Baltic Sea, we also find several locations with > 3 cm differences in the amplitude estimates, but there are no notable discrepancies in the tide gauge records, many of which have been used in previous studies of the SSLC (e.g., Hunicke & Zorita, 2008; Barbosa et al., 2016); after carefully assessing the data quality those tide gauges were retained. This process leads to a final set of 663 tide gauges, for which we use the results from the robust fit approach for further analysis.

Calafat et al. (2018) studied the SSLC in the US Gulf and Atlantic coasts proposing a Bayesian method as an alternative to a harmonic analysis. Under certain conditions, the Bayesian method is more robust in capturing fluctuations, but it is also much more computationally demanding, especially for our global tide gauge analysis. After testing it for several stations, we find that the differences in the results are small (not shown) and do not affect our overall conclusions and hence we proceed with the simpler regression method.

3.2.2 Jackknife Resampling

The next sensitivity test we apply is jackknife resampling on the 5-year moving windows. For each 5-year window we remove data from one year and fit the model, then remove the next year's data and fit the model, and so on, until all 5 years in the window were discarded. This gives for each time step five different estimates of the amplitudes and phases. At each tide gauge, we quantify the spread of the resampling results by calculating the range between the five different estimates of all model components. From this, we obtain a resampling-range value for each time step (i.e., every month). Next, we find the median resampling-range value for each tide

gauge over time. For the annual amplitude component, we find that the median range of resampling results varies from 8 mm to 56 mm across tide gauge locations, with a median value of 18 mm and a standard deviation of 9 mm. From these results and previous literature (Tsimplis & Woodworth, 1994; Plag & Tsimplis, 1999; Amiruddin et al., 2015), we confirm that choosing a 5-year time window for the harmonic analysis is a reasonable choice.

3.2.3 Phase Precision Testing

We produce 700 synthetic 5-year-long time series (to hypothetically represent 700 different tide gauge locations) of daily values of an annual sinusoid with known randomized phase. Then, we compute monthly averages from the daily values. We apply the harmonic analysis to these monthly time series to determine a phase estimate. To compute the error in estimation we take the difference between the estimated phase and the true phase that was initially input to create the synthetic data. From the distribution of 700 time series we incur an error in the phase estimates between 0 and 1.2 degrees different than the true phases. This shows that our model reliably estimates the phases at daily resolution despite the monthly resolution of the input data.

3.3 Quantifying Changes in Amplitude

From the moving harmonic analysis, we obtain time series of the MSL annual and semi-annual amplitudes. In this study we focus solely on changes in the annual amplitude because it is the dominant factor in most locations, apart from the tropics and a few sites in Antarctica where there are relatively fewer tide gauges (Vinogradov et al., 2008). Previous regional studies of the SSLC (e.g., Wahl et al., 2014; Calafat et al., 2018) also emphasized the annual component rather than the semi-annual, and in line with those studies the following discussions of amplitude and

phase all refer to the annual component. In a first assessment, we derive the value of the maximum amplitude at all tide gauge locations and identify in which year it occurred. We do this for two time periods: the entire record of the respective tide gauge (for all 663 tide gauges), and the period post-1970 (for 636 tide gauges with data after 1970). We further quantify the relative variability in annual amplitude by deriving the standard deviation and the ratio between the mean amplitude and the maximum amplitude.

To assess long-term changes, we fit a linear trend to the annual amplitude time series of that same subset focusing on the post-1970 period to derive comparable results across sites. The significance of the trends is assessed with a noise experiment. We run the harmonic analysis on synthetic time series generated from a stationary seasonal cycle (using the mean at each tide gauge) and non-seasonal MSL variability representative of each tide gauge location. The latter is derived by fitting a first-order autoregressive (AR1) model to the detrended and de-seasoned MSL time series. We generate 500 synthetic time series which are all combined with the same stationary seasonal cycle. Then, the 5-year running harmonic analysis is performed and 500 trend estimates are derived for each tide gauge, from which we obtain 5-95% confidence levels and assess whether the trend from the actual data falls outside that range. This quantifies whether the estimates obtained could have occurred by chance from a random red-noise process (representing the non-seasonal variability) and an invariant seasonal cycle.

Finally, following Calafat et al. (2018), we also assess changes in the number of 95th percentile threshold exceedances of the amplitude. In combination with the linear trend analysis and the assessment of when the maximum amplitude occurred, this provides additional insights about amplitude changes. We compare the difference between the number of 95th percentile threshold exceedances that occur in the last decade of the record to the number of exceedances in the first

decade post-1970 at tide gauges with at least 20 years of data after 1970 and no more than 10 years of continuous data gaps in that time period (559 tide gauges).

3.4 Changes in Phase

To identify changes in the phase we use circular statistics (Berens, 2009). This method has been used in previous studies to measure the seasonality of flooding (Villarini, 2016; Veatch & Villarini, 2020) and across other scientific fields that apply periodic data such as phases of the moon, wind direction, animal migration paths, neuroscience, criminology, and more (Bowers et al., 2000; Gao et al., 2006; Cochran et al., 2004, etc.). In our study, the phase describes when during the year MSL reaches its maximum. Quantifying phase over different 5-year windows allows us to evaluate whether the peaks of the ASLC for a location have shifted over time. Circular statistics allow the phase to vary continuously across 0 (360) degrees into the next year. For example, in some locations, the ASLC generally peaks between August to September (phase of 210-270 degrees), whereas in others the range spans across calendar years, for instance, November to January (300-30 degrees).

Considering the angular nature of the data, to accurately reflect instances where the range may cross over 0 degrees, we compute the circular standard deviation defined as:

$$s = \sqrt{-2lnR} \quad (3)$$

where R is the resultant vector length (Berens, 2009). R gives a value from 0 to 1 describing a uniform dispersion (0) throughout the polar circle plane, or concentration in one direction (1). In this application, a phase concentrated in one direction (with an R value near 1) implies a stronger

seasonality, meaning the seasonal pattern is more evident of distinct monthly fluctuations, instead of dispersed throughout the months of the year.

3.5 Regional Coherence and Links to Climate Modes

To identify spatial coherence across locations, we apply a clustering algorithm to group tide gauges according to their patterns of ASLC amplitude changes (Li et al., 2021). We use the *k*-means Dynamic Time Warping (DTW) approach via Python's "tslearn" package (Tavenard et al., 2020). *k*-means partitions the data into *k* number of clusters, or groups, based on their similarity (MacQueen, 1967). The similarity is commonly measured by the squared Euclidean distance of the data points, but in this study, we instead use a modification of *k*-means where we apply DTW as the similarity measure because it detects similar patterns in the time series regardless of whether those features are contemporaneous (Aghabozorgi et al., 2015). DTW warps the path between time series by choosing the closest points between the time series based on the Levenshtein distance calculation (Petitjean et al., 2011). Cluster centroids are computed for each resulting group of time series, where the centroid represents an average sequence that is followed by the rest of the time series within the respective cluster via DTW barycenter averaging (DBA). The amplitude time series are scaled to have zero mean and unit variance to disregard the magnitude of the changes, since our goal is to identify regions where relatively high or low values occur (near-)simultaneously. This approach captures flexible similarities and focuses on similar trajectories between the time series, allowing us to cluster according to the shape of the time series rather than the range of the data.

We focus on clustering tide gauges within the North Atlantic basin because of its dense network of tide gauges with long overlapping periods, and thus, we satisfy the requirement of the algorithm to use a consistent time frame across tide gauges. For this analysis, we select the period from 1990 to 2009 to retain a relatively large number of tide gauges with overlapping records and reasonable coverage of the entire North Atlantic coast. To determine the optimal number of clusters we use the elbow curve method as guidance (Camus et al., 2011), where we compute the standard deviation across time series in a cluster as a function of varying numbers of clusters, and we check the tipping point of the curve. For each cluster we compute the percent variance explained (PVE) by the mean time series of the cluster (Rashid et al., 2019). This shows how much of the variability in amplitude is explained by the cluster mean. Here we take the variance of the amplitude time series for each tide gauge in a cluster (scaled with unit variance = 1), subtract the cluster mean from each individual time series, and compute the variance again. The difference between the initial variance and the resulting variance after removing the cluster mean reveals what portion of the variability in amplitude was contributed by the cluster mean. We multiply this value by 100 to obtain the PVE.

Lastly, we perform a correlation analysis of the annual amplitudes from individual tide gauges with anomalies of relevant climate indices during overlapping time periods at tide gauges with records at least 30 years complete after accounting for data gaps. The time series of the climate indices are smoothed with a 5-year running average in order to compare with the results of the harmonic analysis. The significance of the correlation coefficient is assessed at the 90% confidence level by the effective sample size considering autocorrelation (He & Guan 2013; Rashid et al., 2019).

4. Results

4.1 Changes in Amplitude

In agreement with Pugh & Woodworth (2014), the highest mean annual amplitudes, exceeding 20 cm, are found mainly in East Asia and northern Australia (Figure 2a). Small mean amplitude values below 6 cm are distributed throughout the globe including along the east coast of Canada, the west coast of South America, Pacific Islands, and South Africa (Figure 2a). About 95% of the 663 tide gauges analyzed have a mean amplitude below 17 cm, and only 1% above 20 cm. However, approximately 10% reach a maximum amplitude above 20 cm at some point throughout their record, when accounting for non-stationarity. As shown in Figure 2b, these larger maximum amplitudes are located across the Northern Hemisphere and a few in northern Australia.

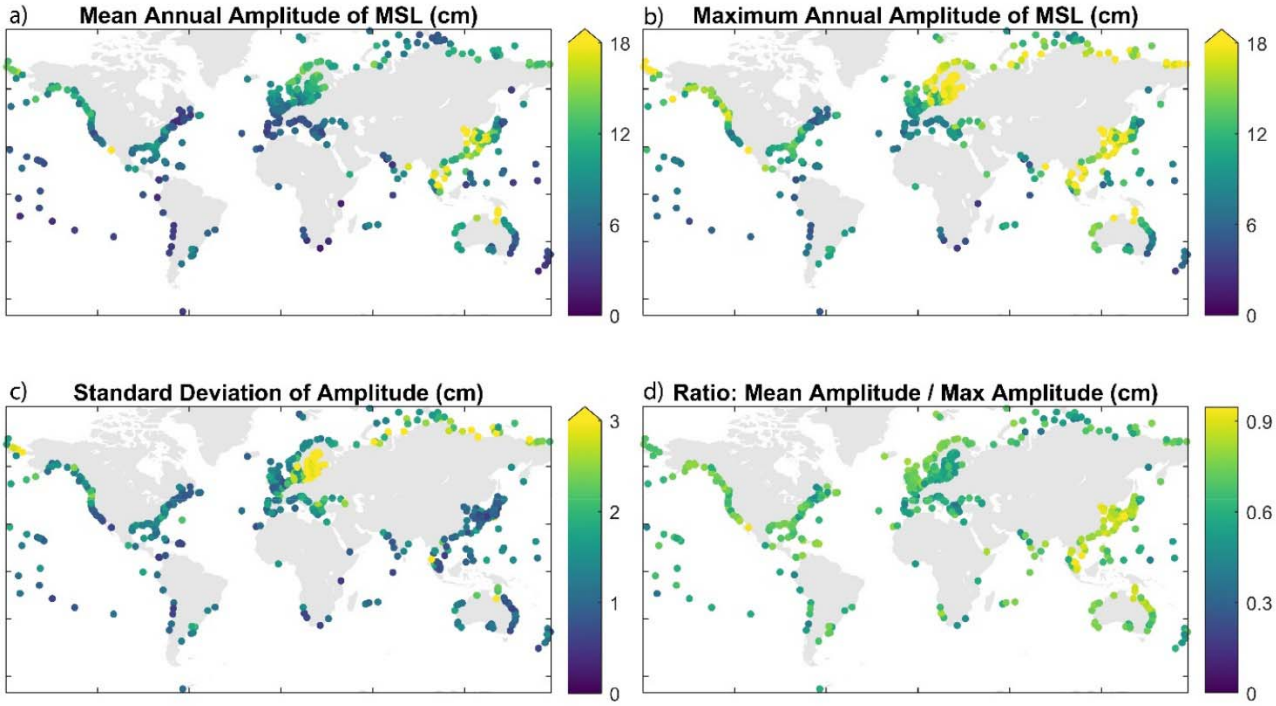

Figure 2. Global maps of annual MSL amplitudes for 663 tide gauges. (a) Mean annual amplitude of MSL (cm). The colorbar is cut off at 18 cm where 26 tide gauges above 18 cm are

shown in yellow. (b) Maximum annual amplitude of MSL (cm) of the entire record where 111 tide gauges with values above 18 cm are shown in yellow. (c) The standard deviation of the annual amplitude. The color bar is cut off at 3 standard deviations where 59 tide gauges with a standard deviation above 3 are shown in yellow. (d) The ratio of the mean annual amplitude to the maximum annual amplitude for each respective tide gauge.

We find that over 75% of the 663 tide gauges' annual amplitudes peak after 1970. When considering only the post-1970 period, over half of the 636 tide gauges with records past that time frame peak after 1990 (Figure 3), and over half in the North American region peak during the most recent decade (after 2010). In northern Europe there is a concentration of peak amplitudes that occur before 1990, while the earliest peaks (1970s) occur in the northern Russian coast and at several other locations around the globe.

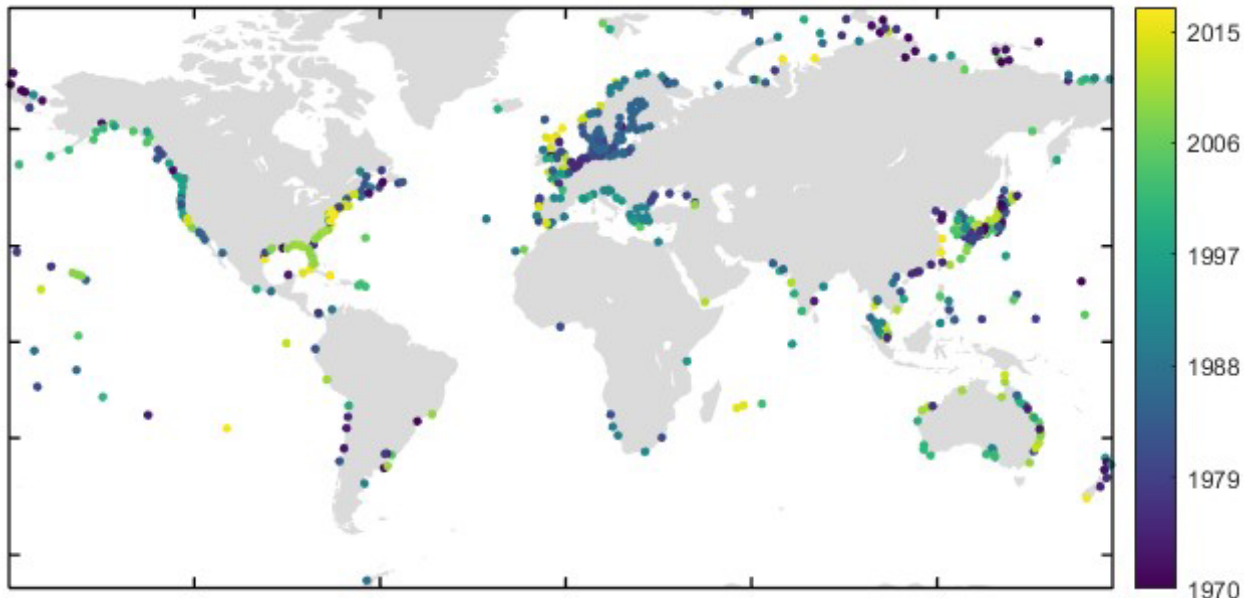

Figure 3. Year when the annual amplitude of MSL peaks for the period post-1970 for 636 tide gauges.

312

313 We consider a subset of 559 tide gauges for the trend analysis (Figure 4a). The subset is
314 composed of tide gauge records that fulfill the following criteria: they cover the period 1970
315 onwards, include more than 20 years of data after 1970, and they have no more than 10 years of
316 continuous data gaps. Significant trends in annual amplitude at the 95% confidence level
317 (according to the noise experiment described in Section 3.3) occur at a total of 125 locations. Out
318 of those, 62 are positive and 63 are negative across the globe. Over 90% of the tide gauges with
319 significant trends show amplitude changes at a rate greater than +/- 0.5 mm/year, and 66 tide
320 gauges greater than +/- 1 mm/year (Figure 4a).

321 At 60 tide gauges, we find that the 95th percentile of the amplitude is exceeded more often during
322 the most recent decade of the records than during the first decade post-1970. In 34 locations,
323 there are more exceedances during the first decade post-1970, and there is no change of
324 exceedances in 31 tide gauges (Figure 4b). Taking Key West as an example, over its entire
325 record, there are 61 out of 1225 months when the annual amplitude exceeds its 95th percentile of
326 about 10 cm; these exceedances all occurred after the year 2000, and 45 of those between 2007
327 and 2011. Neighboring tide gauge stations throughout Florida, Georgia, and the Carolinas also
328 exhibit annual amplitudes exceeding their 95th percentiles during the last decade, but none at the
329 beginning of their records. In Florida, for example, half the tide gauges have over 25 monthly
330 exceedances more during the last decade of available data; the other half show no difference in
331 exceedances between the two periods.

332 Globally (across all regions where tide gauge data are available), the largest difference between
333 the number of exceedances is found along the Gulf of Mexico and east coast of the US with 28
334 more monthly exceedances of the 95th percentile occurring during the most recent decade than

during the 1970s. In contrast, the Baltic experienced higher amplitudes during the 1970s (up to 24 more months exceeding the 95th percentile in Kalix, Sweden) than during the most recent decade in most of their tide gauges. This corresponds with the negative amplitude trends observed in the Baltic. Note that these locations still exhibit significant trends in amplitude over the continuous portion of the record post-1970, although the change is not captured in comparing merely the first and last decades of the post-1970 record. Strong values in both the trend (Figure 4a) and the difference of 95th percentile exceedances (Figure 4b) indicate a continuous trend post-1970, whereas a small trend with a large difference of exceedances between the first and last decades indicates a relatively flat curve (i.e., small trend) with a recent sharp increase (i.e., large difference in 95th percentile exceedances). On the other hand, a strong trend with small difference in exceedances would indicate a continuous increase over much of the record but a recent decline.

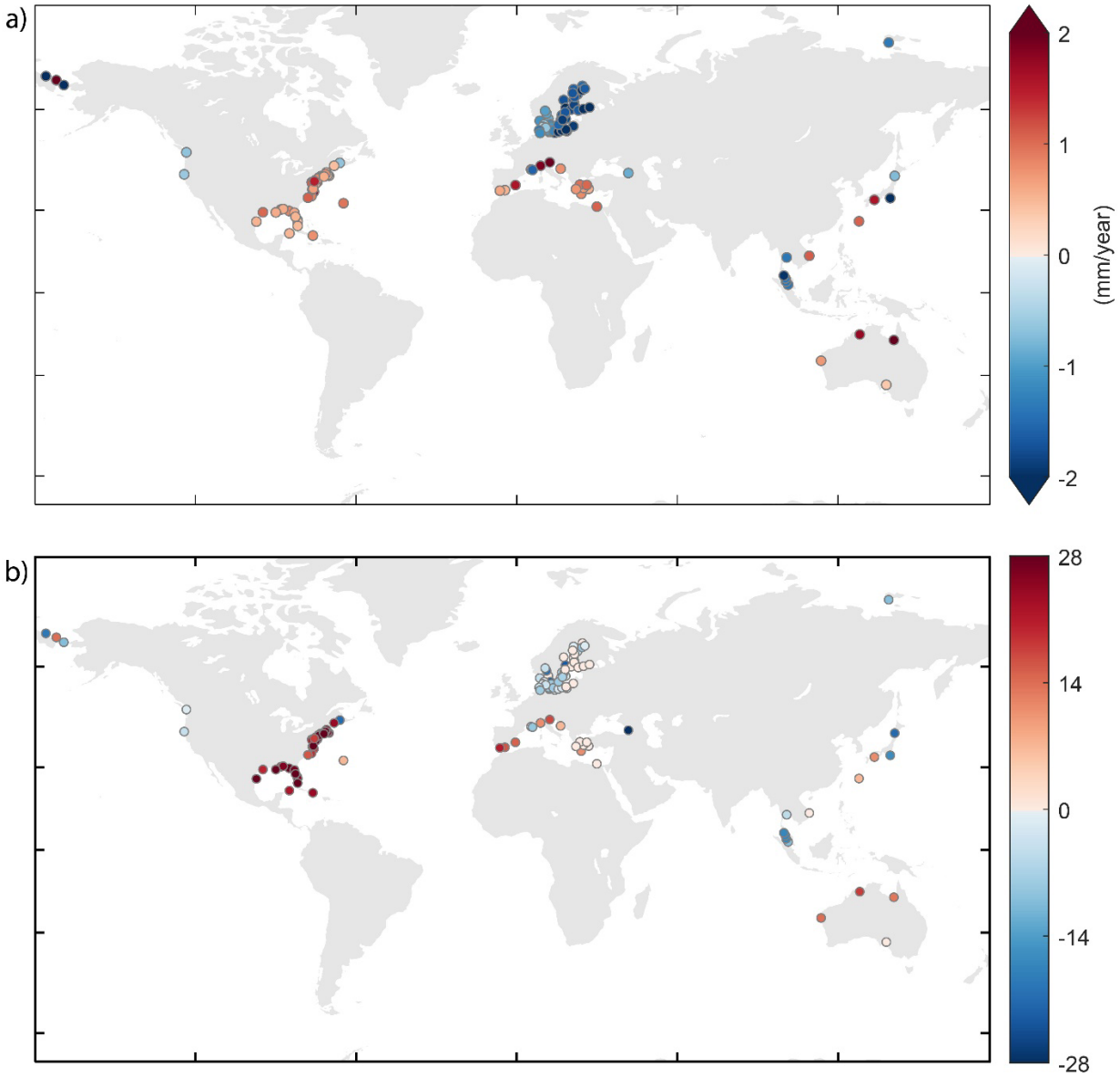

Figure 4. (a) Trends in annual amplitude (mm/year) shown for tide gauges with records at least 20 years long for the period after 1970. Results are shown for 125 tide gauges where trends are significant at the 95% confidence level estimated by the noise experiment. For illustration purposes the color bar is cut off at 2 mm (15 tide gauges have trends with a magnitude over 2 mm). (b) Difference in the number of times (months) that the annual amplitude exceeds its 95th percentile between two time periods: the last decade of the tide gauge record and the first decade of data post-1970. If the difference is positive, it indicates that the annual amplitude exceeded its

355 95th percentile more often during the last decade of the record than during the first decade post-
356 1970.

357 **4.2 Changes in Phase**

358 Globally, the mean annual phases for most tide gauge locations (431 out of 663) indicate an
359 ASLC peak during the fall season of the respective hemisphere, following the time integral of
360 solar heating (September to November for the Northern Hemisphere; March to May for the
361 Southern Hemisphere) (Figure 5a). For the rest of the sites, it peaks during summer in 159 tide
362 gauges, 62 in winter, and 11 in spring. In addition to the mean of the phase, we also assess its
363 variability (Figure 5b) to quantify how dispersed the peaks are during the year.

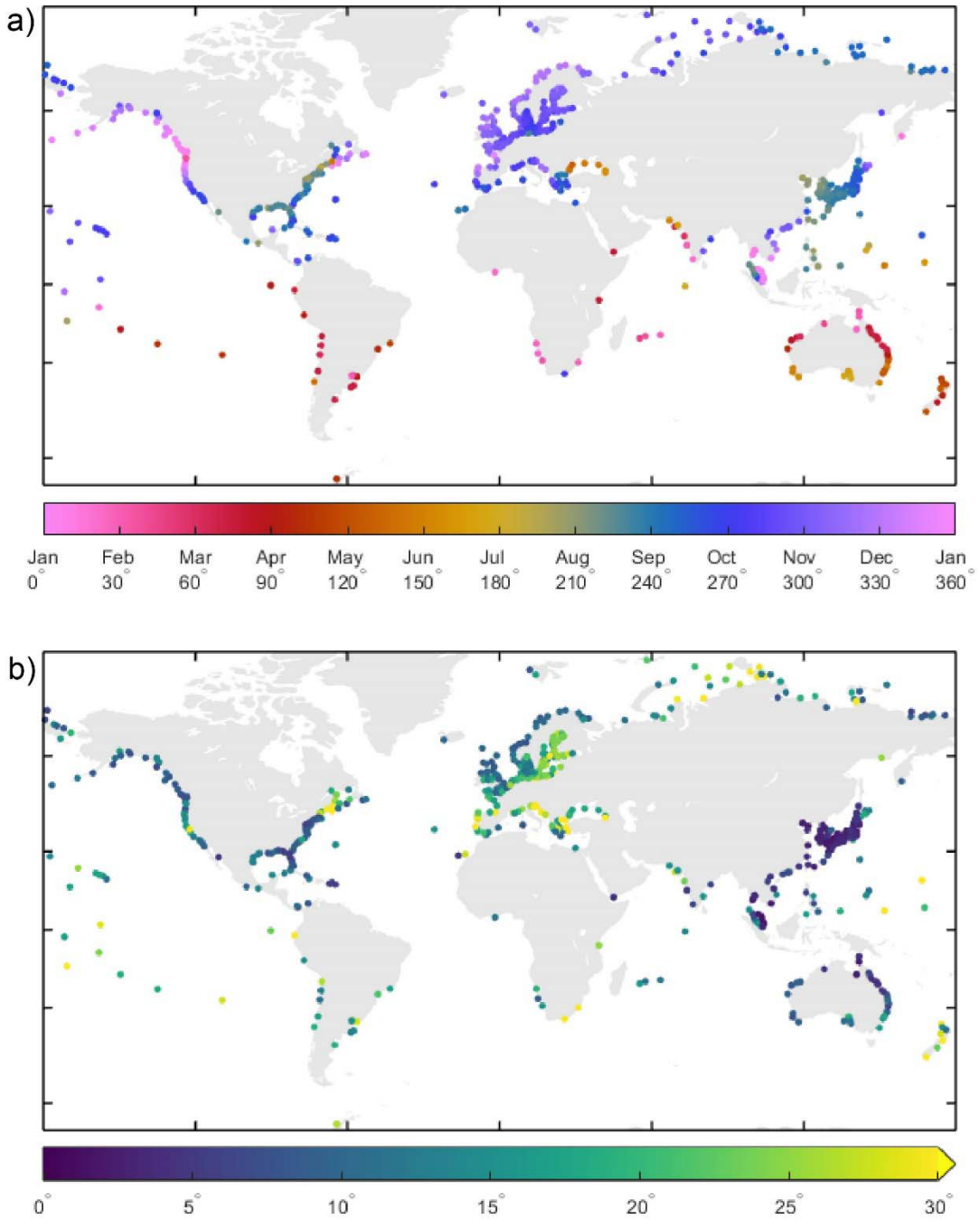

364

365 **Figure 5.** (a) Global map of circular mean annual phase (degrees) where each calendar month is
366 represented by 30-degree increments (b) Circular standard deviation of phase (degrees). The
367 color bar is cut off at 30 degrees where 36 tide gauges with a circular standard deviation above
368 30 degrees (1 month) are shown in yellow.

Recalling that 30 degrees represent approximately one month, regions such as the Mediterranean, Baltic Sea, and the northeast coast of North America are some hotspots where the phase vary most over time (> 30 degrees). For example, Brest (France) has a circular standard deviation value of 23 degrees, and in the Baltic Sea the tide gauge of Swinoujscie (Poland) has a circular standard deviation of 34 degrees. In contrast, the region around Japan exhibits small values between 0 to 5 degrees, indicating that the peak of the annual cycle always occurs around the same time.

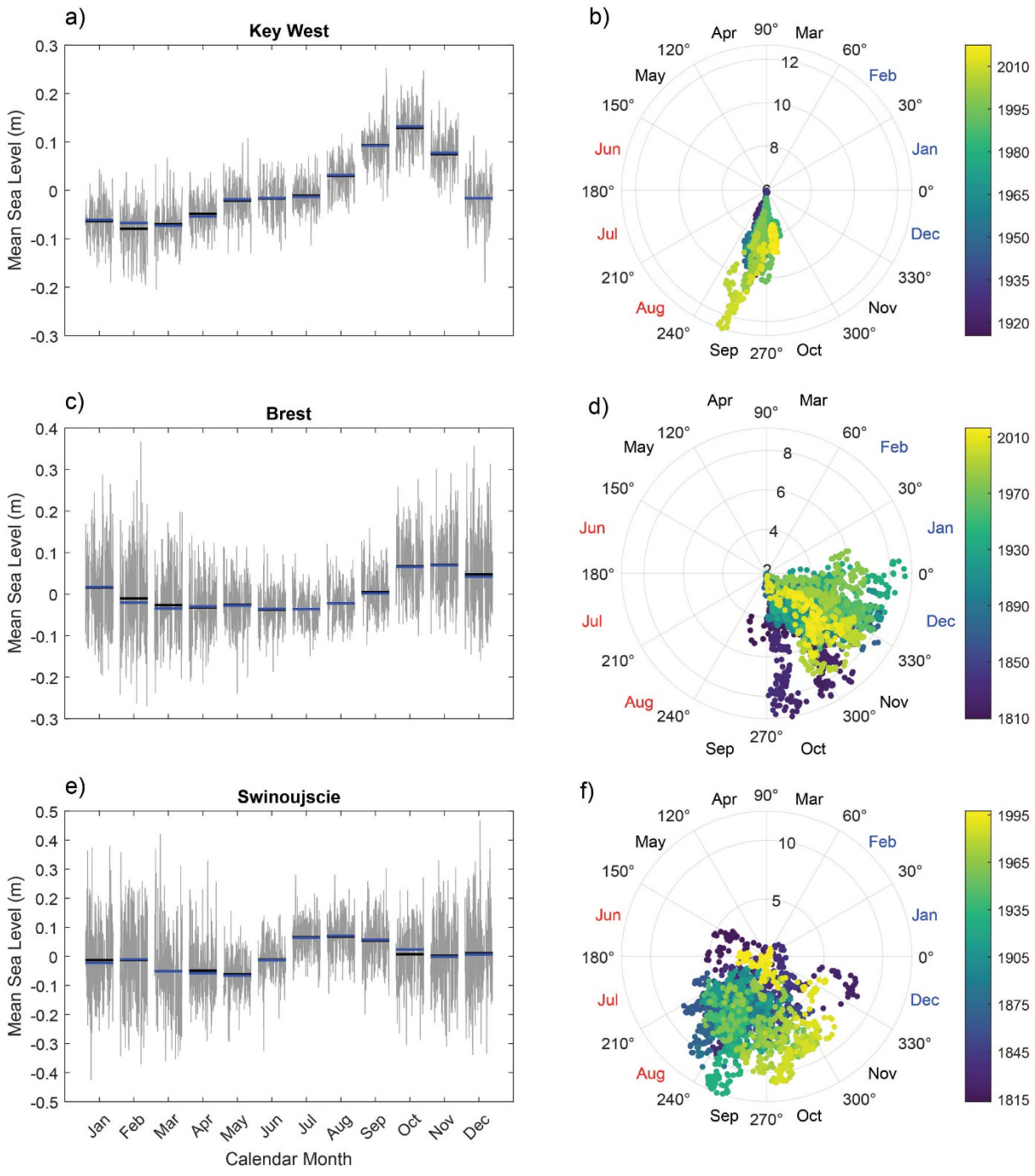

Figure 6. (a) De-trended monthly MSL plotted for each month of the year (grey) for the length of the respective tide gauge record. The black line represents the long-term mean and the blue line represents the median. (b) The month in which the annual phase (degrees) occurs over time. Color bar represents the time step of the record in years. The radius of each circle on the polar

plot represents the annual amplitude (cm). Months in red font represent the summer season and blue font represents the winter season of the respective hemisphere.

In Key West (Florida), the circular standard deviation is also small (8 degrees). At this location, the ASLC peaks between September and October (Figure 6a), and the greater amplitude values (above 10 cm) start to occur after 1993 (Figure 6b). Similarly, in St. Petersburg (western Florida), the phase indicates that the ASLC peaks have shifted from the month of August to September in recent years. Similar results for St. Petersburg were reported in Wahl et al. (2014). Brest (France), on the other hand, typically peaks between October and December, although in recent years, some peaks occurred in January. At the tide gauge of Swinjouscie (Poland), the annual cycle peaks mostly between July to October, but with high variability including peaks across all months of the year (Figure 6c).

4.3 Regional Coherence of Amplitude Changes

The geographic clustering of the time-variable ASLC amplitudes is performed separately for the northwestern and northeastern Atlantic basins, following similar regionalization boundaries as in Enriquez et al. (2020). For this analysis, we use tide gauge records covering the period from 1990 to 2009, resulting in 49 tide gauges in the northwestern and 115 tide gauges in the northeastern Atlantic regions, respectively. As mentioned in Methods, the analysis is restricted to this time period in order to retain the maximum amount of tide gauges with overlapping records and data completeness, while achieving reasonable coverage of the coastline. Note that we include the Mediterranean Sea, but we omit tide gauges located in the Black Sea. After testing

several numbers of clusters suggested by the elbow curve (see Methods), we chose to use 4 clusters for the northwestern and 8 clusters for the northeastern Atlantic regions.

Tide gauges in the northwestern Atlantic region show spatial coherence in the ASLC amplitude time series, especially in the southeastern US and Gulf of Mexico coastlines (Cluster 3 in Figure 7). Similarly, tide gauges north of Cape Hatteras are distinguished as a separate cluster (Cluster 1). Both clusters exhibit an upwards tendency, particularly after 1996. Meanwhile, the amplitude time series of the northernmost tide gauges in Canada (Cluster 4) are less resemblant to their cluster mean (red time series in Figure 7b). In addition to the complexity of the region's bay systems and bathymetry, this is a limitation of the algorithm because it forces every time series to be part of one of the clusters even if it doesn't match the other cluster members well.

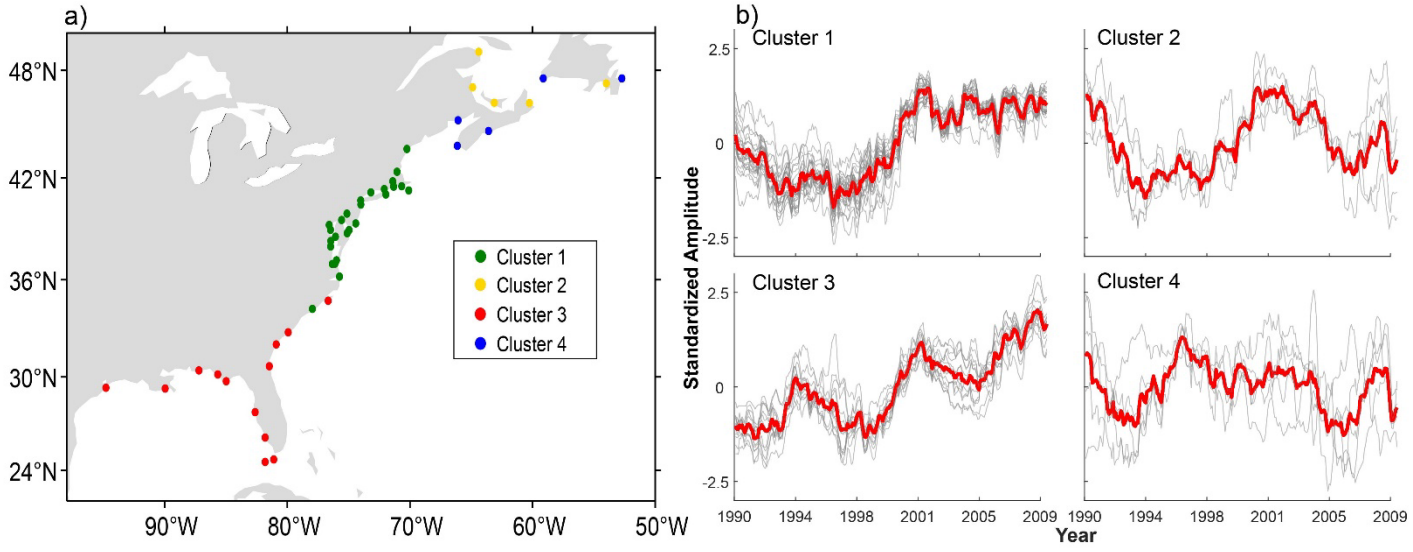

Figure 7. Clustering (*k*-means DTW) annual amplitude time series from the period of 1990 to 2009. (a) Map of 49 tide gauges in the Northwest Atlantic region and the clusters they were assigned. (b) Annual amplitude time series of the individual records within clusters (grey) and the mean cluster time series (red).

In the northeastern Atlantic region (Figure 8), Cluster 4 (green) in the Baltic along the Gulf of Bothnia and Cluster 3 (red) along the Norwegian Sea share similar patterns in their mean cluster time series (Pearson correlation of 0.58); with the northern Baltic gauges (Cluster 4) having more pronounced fluctuations. Cluster 3 (red) coherently groups the ASLC patterns of tide gauges along Norway and the east coast of the United Kingdom (UK). However, three tide gauges grouped into this cluster (orange dots in Figure 9a) are located elsewhere (Vigo and Ceuta in Spain, and Khios in Turkey). Other geographic clusters comprise tide gauges along the southern North Sea (Netherlands, Belgium, France) (Cluster 6), and the complex Skagerrak (Cluster 5) and Kattegat regions (Cluster 2). Cluster 1 is most dispersed geographically (Figure 9a) and in terms of the differences of the time series within the cluster (Figure 9b); it includes tide gauges from the northwestern UK, English Channel, northern Spain, and Adriatic Sea, which may show some similarities within sub-regions but do not fit well into any of the other clusters. Cluster 8 includes a very small number of tide gauges.

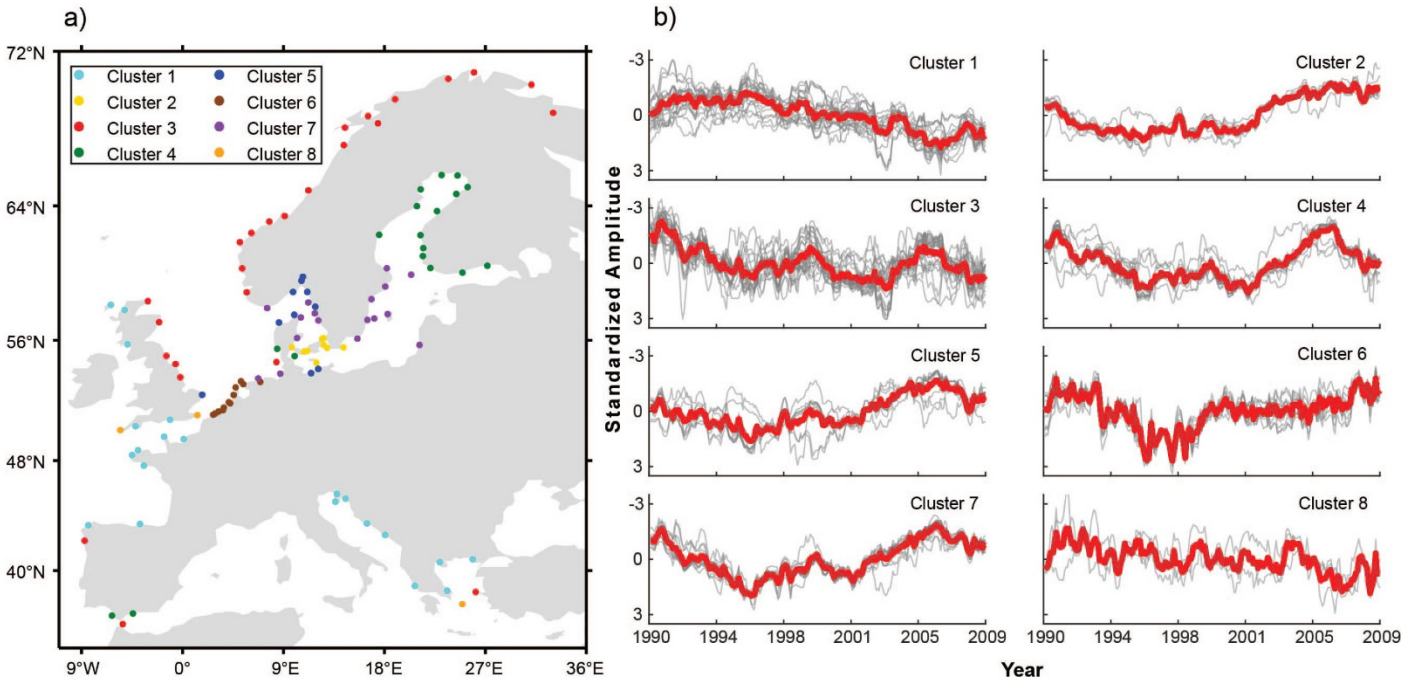

Figure 8. Clustering (*k*-means DTW) annual amplitude time series from the period of 1990 to 2009. (a) Map of 115 tide gauges in the Northeast Atlantic region (Europe) and the clusters they were assigned. (b) Annual amplitude time series of the individual records within clusters (grey) and the mean cluster time series (red).

The percent variance explained (PVE) by each cluster's mean time series (Figure 9) shows how well the cluster mean describes the overall amplitude pattern of the individual tide gauges pertaining to the cluster. Low, near-zero percentages indicate that for certain outlier tide gauges, the mean time series of the cluster (red time series in Figures 7 & 8) does not explain the amplitude variability at those locations. In the Northwest Atlantic the median PVE of Cluster 1 (north of Cape Hatteras) is the highest (92%), as the mean cluster time series explains 67% to 97% of the variance of the individual time series in the cluster. Cluster 4 has the lowest median value (52%) and only explains between 0% to 65% of the variability of the individual time series.

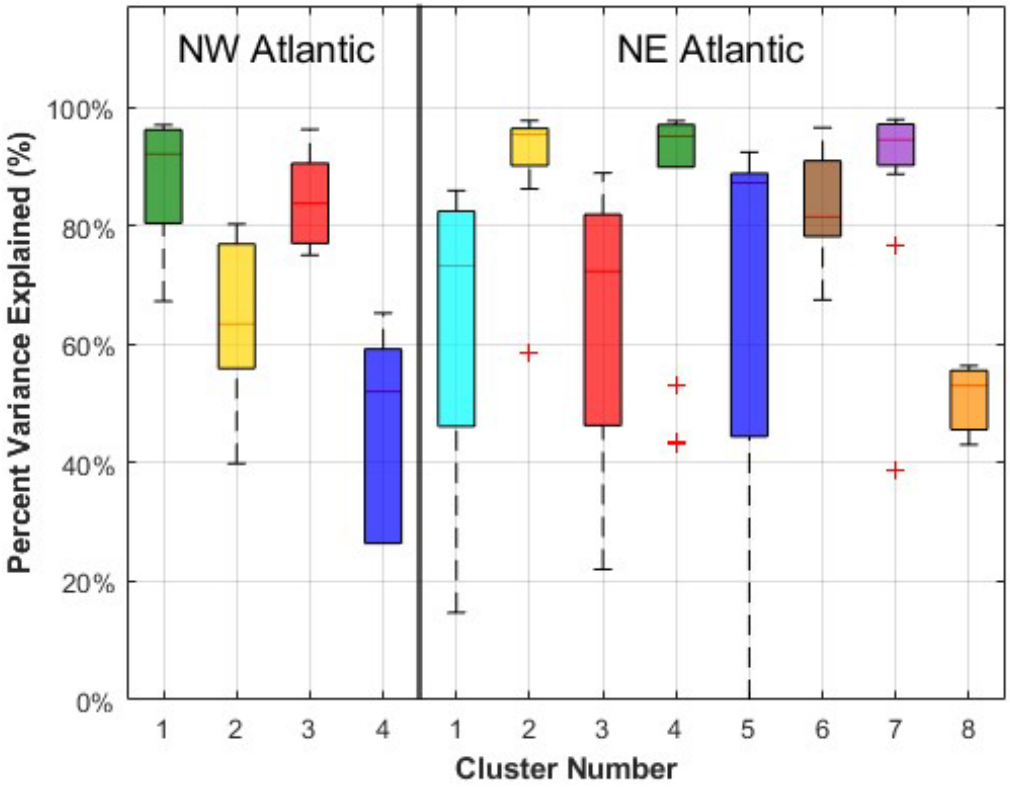

Figure 9. Boxplots of the percent variance explained (PVE) by the mean time series of each cluster. The colors of the boxes match the cluster to which it pertains on the maps in Figures 7a and 8a; the horizontal red lines are the medians, the red crosses (+) are outliers, and the bottom and top edges of each box represent the 25th and 75th percentiles.

For the Northeast Atlantic, clusters 2, 4, and 7 all have high median values and a small spread, indicating that the variability of all time series within the clusters is well explained by the mean cluster time series. Cluster 6 also has a relatively high median but a wider spread, whereas Cluster 8 has a low median value but also a low spread (likely due to the small number of tide gauges in this cluster). Clusters 1, 3, and 5 all show a very large spread, while the median values are also relatively high, especially for cluster 5.

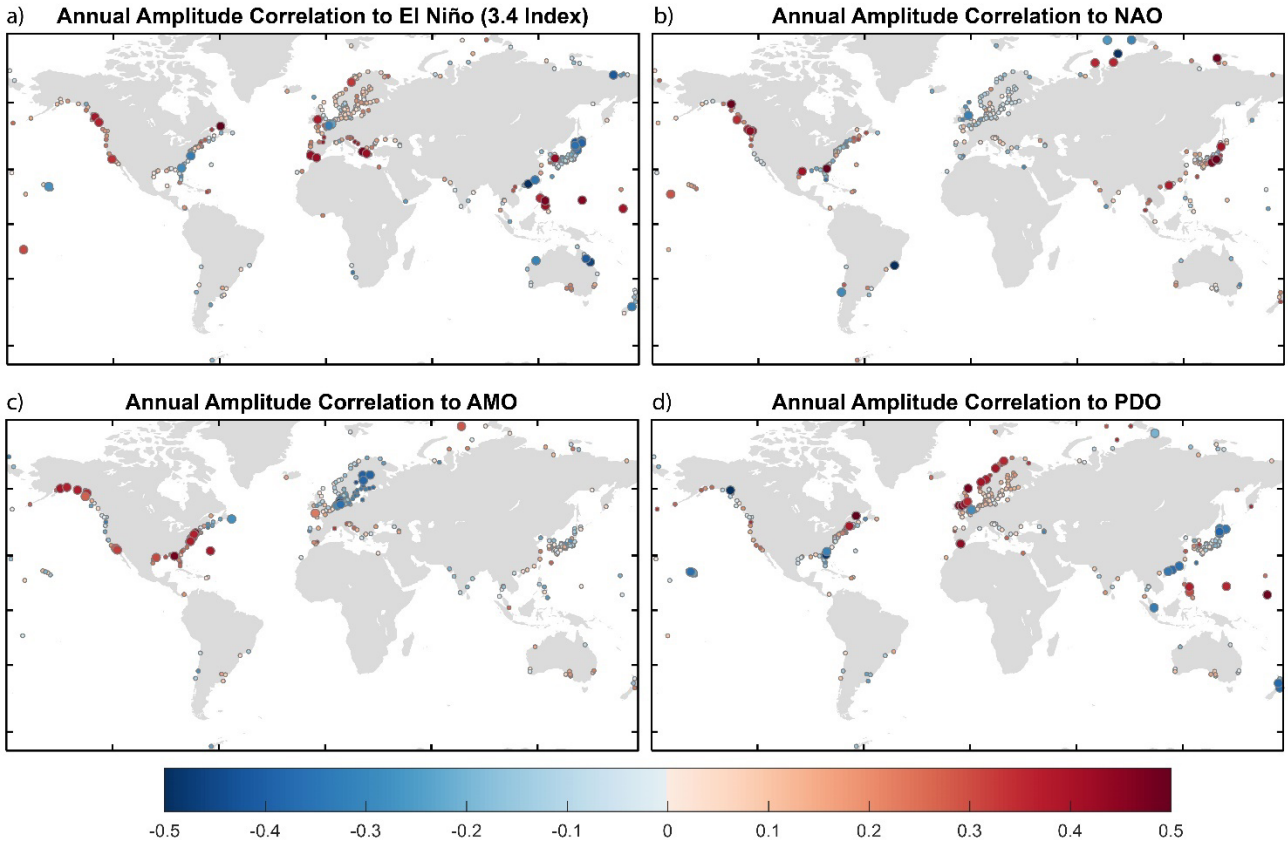

460

461 **Figure 10.** Correlation of annual amplitude to anomalies of climate indices for the overlapping
462 time periods with at least 30 years of full data coverage. Smaller dots represent tide gauges
463 whose correlation was not significant at the 90% confidence level according to the effective
464 sample size and autocorrelation (He & Guan 2013). For illustration purposes, the color bar cuts
465 off correlations with a magnitude greater than 0.5.

466

467 In order to link the ASLC amplitude variability to large scale climate variations, we perform
468 comparisons to anomalies of relevant climate indices (smoothed with a 5-year running mean for
469 comparison with the results of the running harmonic analysis) by computing the correlation
470 coefficient for overlapping time periods when those are at least 30 years long (Figure 9). The El
471 Niño 3.4 Index correlates significantly with the ASLC amplitude changes at 36 out of the 423

tide gauges. In the northeastern Pacific there is strong positive correlation (up to 0.5 correlation coefficient) with tide gauges on the western US coast. The NAO, AMO, and PDO show significant correlations at 24 out of 326, 27 out of 328, and 36 out of 328 tide gauges, respectively. The NAO and AMO correlate positively with the annual amplitudes at tide gauges in the western coast of North America. The AMO also correlates positively with tide gauges on the eastern coast of the US, and negatively with those in the Baltic Sea. The PDO shows coherent positive correlation along the coast of the Norwegian Sea.

5. Discussion

Previous literature has documented the amplitude of the seasonal cycle in MSL for different parts of the world. This analysis goes further (focusing on the ASLC) to investigate those changes over time for the entire global coast where tide gauge data is available. From assessing the mean SSLC globally, Pugh & Woodworth (2014) display comparable amplitude and phase outputs resulting from a harmonic analysis of tide gauges in the same dataset (PSMSL) that we use in the present study. Vinogradov et al. (2008) studied the SSLC's amplitudes and phases globally including the open oceans using satellite data; they focused on the climatological means of a 13-year period. Their estimates differ slightly from ours; for example, most amplitude values they found were < 10 cm, (in a few cases reaching 15 cm), whereas we find that 95% of the tide gauges have mean amplitudes of 17 cm or more (with several locations over 20 cm). This indicates that altimetry data may underestimate the SSLC amplitudes along the coast, especially because their study does not consider barometric pressure effects and the inverted barometer. Our data still retain air pressure effects, which may explain some of the differences, particularly at higher latitudes (Ponte, 2006). However, the general spatial patterns are consistent in that we

observe relatively higher amplitude values in the Western Pacific, specifically in regions like East Asia and Northern Australia.

Wahl et al. (2014) used the same approach as we do here to assess non-stationarity for the US Gulf Coast where they compared the amplitude changes pre- and post-1990s. In our study we highlight the time periods of the first decade containing data post-1970 and the last decade of each respective tide gauge record. For the South China Sea, Amiruddin et al. (2015) explored the temporal variability in the SSLC and found some high variability in the annual amplitudes, which coincides with our results showing that some locations in this region can reach up to 2.8 standard deviations from their annual amplitude. Annual amplitudes have varied over time at most of our study locations. At over 75% of all the tide gauges analyzed, the maximum amplitudes occurred after 1970, with a tendency to peak during the most recent decade in North America. Small ratios of mean to maximum ASLC values reveal locations where amplitude changes are more apparent. For example, the smallest ratios are found in Alexandroupolis within the Mediterranean Sea, Pago Pago, Midway Island and La Libertad II in the Pacific, and Dikson and Fedorova in Russia where we speculate influences by changes in seasonal ice cover (Ruiz Etcheverry et al., 2014).

Our estimates of circular mean annual phase indicate that for most of the tide gauges in our global analysis, the ASLC peaks during the fall season, which overlaps with the most active storm seasons in the Pacific and Atlantic basins (Oey et al., 2016; Roustan et al., 2022). To identify where the phase deviates from its mean over time, we map the circular standard deviation of the phase (Figure 5b). We notice several regions that exhibit a high circular standard deviation such as the Mediterranean, Baltic, some Pacific Islands, and the northeastern coast of North America. The latter region includes several tide gauges located in river mouths or

518 (complex) bay systems where river runoff can influence the seasonal cycle (Pugh & Woodworth,
519 2014). For instance, the tide gauge at Bar Harbor in Frenchman Bay, Maine (circular standard
520 deviation of 32.3 degrees) exhibits a phase shift from May to October in the beginning of the
521 record but is more concentrated from June to August past the 1980s and has remained between
522 July and August after the late 1990s. This region of high deviation is one of comparatively low
523 mean amplitude values (around 6 cm or less).

524 Another extreme example with a very dispersed phase (circular standard deviation of 34 degrees)
525 is Swinoujscie, Poland, where peaks have occurred during every month of the year at some point
526 in the record; although most of those peaks are observed during July, August, and September. In
527 general, we find that locations with a higher circular standard deviation of the phase have a less
528 pronounced seasonal cycle (Dunne et al., 2012) and contain more interannual variability in the
529 ASLC amplitude. Locations with a more discernable seasonal pattern (e.g., Japan, Key West,
530 etc.) have less deviation in their phase. For example, locations where the ASLC is not very
531 pronounced are found in the Mediterranean, specifically in Greece, and also in the Pacific Island
532 of Pago Pago, and South Africa. Locations of high standard deviation (where the phase spreads
533 out around a month or more) are scattered around the globe but most commonly found in (semi-
534)enclosed basins, Pacific Islands, and near bays. Large circular standard deviation values are also
535 found in Russia, which is a distinct region due to its proximity to the poles.

536 From our cluster analysis (Figure 8), tide gauge stations along the southeast US coast (Cluster 3)
537 and those north of Cape Hatteras (Cluster 1) show increasing ASLC amplitudes after the 1990s,
538 with trends of 0.5 mm/year or more. For example, in Key West FL, the amplitude values did not
539 surpass 10 cm until 1993. For the southeast US similar results were reported in Calafat et al.
540 (2018). More than 90% of the 125 tide gauges with significant trends post-1970 show amplitude

changes at a rate of +/- 0.5 mm/year or more. Figure 4a shows strong negative trends for locations in the Baltic Sea where the annual amplitude is decreasing more than 2 mm/year in some parts. Hunicke and Zorita (2008) find increasing trends in the amplitude in their study of the Baltic Sea, but they analyzed the entire 20th century whereas our trend analysis takes data from the 1970s onwards, including more recent data than was available at the time of their study. While annual amplitudes in the Baltic have followed an increasing centennial trend, it turned negative for the last several decades. Although the amplitude was found to have changed over time, the phase has remained relatively stable in the Baltic. That is, as reported by Hunicke and Zorita (2008), low peaks occur in spring months and high peaks in winter which aligns with our findings. They also point out the Gulf of Bothnia (our Cluster 4 in the European region shown in Figure 9) as having higher interannual and decadal variability than the rest of the Baltic, which explains the more distinct fluctuations in the Cluster 4 amplitude time series as compared to the southern Baltic gauges belonging to Cluster 7. Tide gauges in the Baltic showed no significant correlation in their annual amplitudes related to the rest of the climate indices tested except for significant negative correlation to the AMO.

When clustering the northwestern Atlantic region post-1990, we find strong regional coherence among Cluster 1 and Cluster 3, located to the north and south of Cape Hatteras, respectively. Their cluster means explain over 95% of the variances in the annual amplitude time series of the tide gauges clustered. While both show increasing amplitudes, the variability is different, as also reported by Calafat et al. (2018). Cape Hatteras is the point where the Gulf Stream detaches from the coast, and Woodworth et al. (2014), for example, suggest wind-forcing and the Atlantic Meridional Overturning Circulation (AMOC) to play a role in the distinction of MSL variability in the regions north and south of Cape Hatteras on decadal timescales. Notably, the AMO Index

reached a positive phase after the 1990s, indicating anomalously higher sea surface temperatures in the North Atlantic basin during the time period of our clustering, which affects thermal expansion of the water column in the region and could be a possible contributor to the ASLC changes we find. Along the North Atlantic coast of the US we find positive correlations between the annual amplitudes and the AMO index, while in the Baltic Sea we find negative correlations during the overlapping time periods. A more detailed attribution of the observed changes to physical processes is beyond the scope of this study.

6. Conclusions

We performed a global coastal ASLC analysis. Using a harmonic regression and clustering methods, we assessed mean values for the ASLC components and quantified changes over time, identifying hotspots where either amplitude or phase changes were most pronounced. Globally, we find higher mean annual amplitudes along the coasts of the Pacific and Indian Ocean. In such places, the ASLC plays a significant role in local seasonal sea level variability. Changes in the ASLC amplitude feature spatial variability across the globe, but when focusing on the North Atlantic we find coherent variations in individual regions especially on the east coast of the US. Changes in the annual amplitude over time were significant (according to a noise experiment) in 125 locations, with both negative and positive trends.

In addition to the annual amplitudes, we also assessed the variability in the annual phases and found that the peaks in sea level tend to occur during the fall season of the year for the respective hemispheres, but some tide gauge locations exhibit strong variability or long-term changes in the phase over time. For example, tide gauge sites in the Pacific Islands and in the Mediterranean have phases dispersed throughout many months of the year. Both changes reported here in terms

of annual amplitude and phase can lead to higher base water levels on which storm surges or extreme waves can be superimposed, thereby leading to increased flooding risk. Finally, we also link changes in the ASLC amplitudes to climate indices such as the AMO which is negatively correlated with tide gauges in the Baltic Sea. ASLC variations in the deep ocean differ from those in shallow water (Pugh & Woodworth, 2014) analyzed here. Therefore, it is of interest to extend our analysis of the ASLC beyond coastal tide gauges by incorporating satellite altimetry and ocean model data to fully capture the global behavior of the ASLC. Based on the results presented and discussed here, future research steps could include (1) using model experiments to identify the underlying mechanisms of ASLC variation; (2) incorporating offshore locations in understanding ASLC patterns and their seasonal changes globally; (3) linking the MSL seasonality patterns to the other extreme sea level oceanographic components such as ocean wave and storm surge events (Reinert et al., 2021); and (4) linking ASLC and extreme sea level variability to atmospheric patterns and drivers at multiple timescales.

Acknowledgements

This research was supported by NASA's Sea Level Change Science Team (grant 80NSSC20K1241). A.B. was funded by University of Central Florida's McNair Graduate Scholar Fellowship. A. Enríquez was funded by Marie Skłodowska-Curie Actions, project 101019470 – SpaDeRisks. J.M. acknowledges support of the University of Central Florida (UCF) Pre-eminent Postdoctoral Program (P3). S.D. also acknowledges David and Jane Flowerree for their endowment funds.

Data Availability Statement

The monthly MSL data used for harmonic analysis are available at PSMSL's website: https://psmsl.org/data/obtaining/. The climate indices used for comparison with the sea level annual amplitudes are available at NOAA's Physical Sciences Laboratory: https://psl.noaa.gov/data/climateindices/list/#Nina34.

References

Aghabozorgi, S., Shirkhorshidi, A. S., & Te Ying, W. (2015). Time-series clustering: A decade review. *Information Systems 53*, 16–38. https://doi.org/ 10.1016/j.is.2015.04.007

Amiruddin, A. M., I. D. Haigh, M. N. Tsimplis, F. M. Calafat, and S. Dangendorf (2015). The seasonal cycle and variability of sea level in the South China Sea, *Journal of Geophysical Research: Oceans, 120,* 5490–5513. https://doi:10.1002/ 2015JC010923

Barbosa, S. M., & Donner, R. V. (2016). Long-term changes in the seasonality of Baltic sea level. *Tellus, Series A: Dynamic Meteorology and Oceanography*, *68*(1). https://doi.org/10.3402/tellusa.v68.30540

Barbosa, S. M., and M. E. Silva (2009), Low-frequency sea-level change in Chesapeake Bay: changing seasonality and long-term trends, Estuarine Coastal Shelf Sci., 83, 30–38, doi:10.1016/j.ecss.2009.03.014.

631 Barbosa, S. M., M. E Silva, and M. J. Fernandes (2008). Changing seasonality in North Atlantic
632 coastal sea level from the analysis of long tide gauge records, *Tellus A*, 60, 165–177.
633 https://doi.org/10.1111/j.1600-0870.2007.00280

634

635
636 Berens, P. (2009). CircStat: A MATLAB Toolbox for Circular Statistics. *Journal of Statistical*
637 *Software*, *31*(10), 1–21. https://doi.org/10.18637/jss.v031.i10

638

639 Bowers J.A., Morton I.D., & Mould, G.I. (2000). Directional Statistics of the Wind and Waves.
640 *Applied Ocean Research*, 22(1), 13–30.

641

642 Calafat, F. M., Wahl, T., Lindsten, F., Williams, J., & Frajka-Williams, E. (2018). Coherent
643 modulation of the sea-level annual cycle in the United States by Atlantic Rossby waves. *Nature*
644 *Communications*, *9*(1), 2571. https://doi.org/10.1038/s41467-018-04898-y.

645

646 Camus, P., Mendez, F. J., Medina, R., & Cofiño, A. S. (2011). Analysis of clustering and selection
647 algorithms for the study of multivariate wave climate. *Coastal Engineering* (Vol. 58, Issue 6, pp.
648 453–462). https://doi.org/10.1016/j.coastaleng.2011.02.003

649

650 Cochran, W.W., Mouritsen, H., & Wikelski, M. (2004). Migrating Songbirds Recalibrate Their
651 Magnetic Compass Daily from Twilight Cues. *Science, 304*, 405 - 408.
652 https://doi.org/10.1126/science.1095844

Dangendorf, S., Wahl, T., Hein, H., Jensen, J., Mai, S., Mudersbach, C. (2012). Mean Sea Level variability and influence of the North Atlantic Oscillation on long-term trends in the German Bight, *Water, 4*(1), 170-195, https://doi.org/10.3390/w4010170

Dangendorf, S., Wahl, T., Mudersbach, C., Jensen, J. (2013). The seasonal mean sea level cycle in the south-eastern North Sea, *Journal of Coastal Research,* Special Issue No. 65, pp. 1915-1920, ISSN 0749-0208. https://doi.org/10.2112/SI65-324.1

Dunne, R.P., Barbosa, S.M. and Woodworth, P.L. (2012). Contemporary Sea Level in the Chagos Archipelago, Central Indian Ocean. *Global and Planetary Change*, 82-83, 25-37. https://doi.org/10.1016/j.gloplacha.2011.11.009

Feng, X., Tsimplis, M. N., Marcos, M., Calafat, F. M., Zheng, J., Jorda, G. and Cipollini, P. (2015*)* Spatial and temporal variations of the seasonal sea level cycle in the northwest Pacific. *Journal of Geophysical Research: Oceans*, 120 (10). pp. 7091-7112. ISSN 2169-9291 doi: https://doi.org/10.1002/2015JC011154

Gao, F., Chia, K.-S., Krantz, I., Nordin, P. & Machin, D. (2006). On the application of the von Mises distribution and angular regression methods to investigate the seasonality of disease onset. *Statistics In Medicine*., 25: 1593-1618. https://doi.org/10.1002/sim.2463

673 Gill, A.E., Niller, P. (1973). The theory of the seasonal variability in the ocean. *Deep Sea*
674 *Research and Oceanographic Abstracts* 20, 141-177.

675

676 He, X., & Guan, H. (2013). Multiresolution analysis of precipitation teleconnections with large-
677 scale climate signals: A case study in South Australia, *Water Resources Research*, 49, 6995–
678 7008. https://doi.org/10.1002/wrcr.20560.

679

680 Holgate, S. J., Matthews, A., Woodworth, P. L. et al. (2013). New data systems and products at
681 the Permanent Service for Mean Sea Level. *Journal of Coastal Research*, 29, 493–504,
682 doi:10.2112/JCOASTRES-D-12-00175.1

683

684 Hünicke, B., and E. Zorita (2008). Trends in the amplitude of Baltic Sea level annual cycle,
685 *Tellus Ser. A*, 60, 154–164, doi:10.1111/j.1600-0870.2007.00277.

686

687 IPCC, 2023: *Climate Change 2023: Synthesis Report.* A Report of the Intergovernmental Panel
688 on Climate Change. Contribution of Working Groups I, II and III to the Sixth Assessment Report
689 of the Intergovernmental Panel on Climate Change [Core Writing Team, H. Lee and J. Romero
690 (eds.)]. IPCC, Geneva, Switzerland, (in press)

691

692 Ku, H. H. (1966). Notes on the use of propagation of error formulas. *J. Res. National Bureau of*
693 *Standards* 70, 263–273.

694

Li, S., Wahl, T., Talke, S.A., Jay, D.A., Orton, P.M., Liang, X., Wang, G., Liu, L. (2021). Evolving tides aggravate nuisance flooding along the United States coastline. *Science Advances*. 7(10), eabe2412. https://doi.org/10.1126/sciadv.abe2412

Li, K., Sward, K., Deng, H., Morrison, J., Habre, R., Franklin, M., Chiang, Y., Ambite, J.L., Wilson, J.P., Eckel, S.P. (2021). Using dynamic time warping self-organizing maps to characterize diurnal patterns in environmental exposures. *Scientific Reports* 11, 24052. https://doi.org/10.1038/s41598-021-03515-1

Marcos, M., & Tsimplis, M. N. (2007), Variations of the seasonal sea level cycle in southern Europe, J. Geophys. Res., 112, C12011, doi:10.1029/2006JC004049.

Newey, W. K., and K. D. West (1987). A simple, positive semi-definite, heteroskedasticity and autocorrelation consistent covariance matrix, *Econometrica*, 55(3), 703– 708. https://doi.org/10.2307/1913610

Oey, L.-Y. & Chou, S. (2016). Evidence of rising and poleward shift of storm surge in western North Pacific in recent decades. *Journal of Geophysical Research: Oceans* 121, 5181–5192. https:// doi.org/ 10.1002/2016JC011777.

Pattullo, J., Munk W., Revelle R., & Strong, E. (1955). The Seasonal Oscillation in Sea Level, *Journal of Marine Research* 14, 88–155

716

717 Petitjean, F., Ketterlin, A., & Gançarski, P. (2011). A global averaging method for dynamic time
718 warping, with applications to clustering. *Pattern Recognition*, *44*(3), 678–693.
719 https://doi.org/10.1016/J.PATCOG.2010.09.013

720

721 Plag, H.-P.; Tsimplis, M.N. (1999). Temporal variability of the seasonal sea-level cycle in the
722 North Sea and Baltic Sea in relation to climate variability. *Global and Planetary Change* 20,
723 173–203 https://doi.org/10.1016/S0921-8181(98)00069-1

724

725 Ponte, R.M., (2006). Low-frequency sea level variability and the inverted barometer effect.
726 *Dynamics of Atmospheres and Oceans* 23 (4), 619–629. https://doi.org/10.1175/ JTECH1864.1

727

728 Rashid, M.M., Wahl, T., Chambers, D.P., Calafat, F.M., & Sweet, W.V. (2019). An extreme
729 sea level indicator for the contiguous United States coastline, *Nature Scientific*
730 *Data,* 6, 326, https://doi.org/10.1038/s41597-019-0333-x

731

732 Reinert, M., Pineau-Guillou, L., Raillard, N., & Chapron, B. (2021). Seasonal shift in storm
733 surges at Brest revealed by extreme value analysis. *Journal of Geophysical Research: Oceans*,
734 *126*, e2021JC017794. https://doi. org/10.1029/2021JC017794

735

736 Roustan, J. B., Pineau-Guillou, L., Chapron, B., Raillard, N., & Reinert, M. (2022). Shift of the
737 storm surge season in Europe due to climate variability. *Scientific Reports*, *12*(1), 1-11.
738 https://doi.org/10.1038/s41598-022-12356-5

739

740 Ruiz Etcheverry, L. A., Saraceno, M., Piola, A. R., Valladeau, G., & Möller, O. O. (2015). A
741 comparison of the annual cycle of sea level in coastal areas from gridded satellite altimetry and
742 tide gauges. *Continental Shelf Research*, *92*, 87–97. https://doi.org/10.1016/J.CSR.2014.10.006

743

744 Smith, J. M. K., Cialone, M. A., Wamsley, T. V., & McAlpin, T. O. (2010). Potential impact of
745 sea level rise on coastal surges in southeast Louisiana. *Ocean Engineering*, *37*(1), 37–47.
746 https://doi.org/10.1016/j.oceaneng.2009.07.008

747

748 Tavenard, R., Faouzi, J., Vandewiele, G., Divo, F., Androz, G., Holtz C., Payne, et al. (2020).
749 Tslearn, A Machine Learning Toolkit for Time Series Data, *Journal of Machine Learning*
750 *Research*, 21(118), 1−6, 2020

751

752 Torres, R. R., & Tsimplis, M. N. (2012). Seasonal sea level cycle in the Caribbean Sea, *Journal*
753 *of Geophysical Research: Oceans*, 117, C07011. https://doi.org/10.1029/2012JC008159

754

755 Tsimplis, M.N., & Woodworth, P.L. (1994). The global distribution of the seasonal sea level
756 cycle calculated from coastal tide gauge data. *Journal of Geophysical Research: Oceans 99*:
757 https://doi.org/10.1029/94JC01115

758

759 Veatch, W., & Villarini, G. (2020). Modeling the seasonality of extreme coastal water levels with
760 mixtures of circular probability density functions. *Theoretical and Applied Climatology* 140,
761 1199–1206 https://doi.org/10.1007/s00704-020-03143-1

762

763 Villarini, G. (2016). On the seasonality of flooding across the continental United States.
764 *Advances in.Water Resources.* 87, 80–91. https://doi.org/10.1016/j.advwatres.2015.11.009.

765

766 Vinogradov, S. V., Ponte R. M., Heimbach, P., & Wunsch C. (2008). The mean seasonal cycle in
767 sea level estimated from a data-constrained general circulation model, *Journal of Geophysical*
768 *Research: Oceans*, 113, C03032, https://doi.org/10.1029/2007JC004496

769

770 Wahl, T., Calafat, F. M., & Luther, M. E. (2014). Rapid changes in the seasonal sea level cycle
771 along the US Gulf coast from the late 20th century, Geophysical Research Letters, 41.
772 https://doi.org/10.1002/2013GL058777

773

774 Woodworth, P. L., & Player R. (2003). The permanent service for mean sea level: An update to
775 the 21st century, *Journal of Coastal Research,* 19, 287-295.